

Connecting Shear Thinning and Dynamic Heterogeneity in Supercooled Liquids by Localized Elasticity

Ke-Qi Zeng,¹ Dong-Xu Yu,¹ and Zhe Wang^{1,*}

¹*Department of Engineering Physics and Key Laboratory of Particle and Radiation Imaging (Tsinghua University) of Ministry of Education, Tsinghua University, Beijing 100084, China*

(Dated: January 7, 2025)

Dynamic heterogeneity and shear thinning are two universal dynamic phenomena in supercooled liquids, respectively at the microscopic level and the macroscopic level. With simulation, we show that they are quantitatively bridged by localized elasticity embodied as transient clusters that elastically respond to shear. Prominent dynamic heterogeneity emerges right after the massive yielding of these clusters, which is initiated by shear transformation zones and facilitated by elastically mediated interaction. With this picture, a scaling law relating shear thinning to the characteristic length scale of dynamic heterogeneity is found.

Supercooled liquids exhibit remarkable shear thinning when subjected to strong steady shear flow: At high enough shear rates $\dot{\gamma}$, the shear viscosity η decreases with $\dot{\gamma}$ as $\eta \sim \dot{\gamma}^{-\lambda}$ [1, 2]. The microscopic mechanism of this nonlinearity has attracted great scientific interest in the past half century [3–16]. Many approaches seek for structural indicators by characterizing the structural distortion at the pair level [4–12]. These efforts connect the shear thinning to cage configuration [5–9] or the distortion of the pair distribution function $g(\mathbf{r})$ at the spatial range beyond the cage [11, 12]. The second class of approaches tackles this problem by considering the dynamic heterogeneity (DH) [13–16] i.e., dynamic regions where particles collectively undergo nontrivial displacements to rearrange structure [17, 18]. These studies have established a correspondence between the shear thinning and the evolution of DH [13]. Such success is expected considering the importance of DH in the research on the slow dynamics of supercooled liquids. Nevertheless, the relation between the aforementioned two classes of approaches is unclear. More seriously, the micro-mechanical connection between the shear thinning and the dynamic region remains elusive, which impedes the constitutive modeling through DH.

Owing to the extremely viscous feature, deeply supercooled liquids can be viewed as “solids that flow” [19, 20], in the sense that they behave elastically below certain length scales at short time scales. This conceptual picture has been substantiated significantly in recent years [21]. For example, elastic signature is observed in the stress correlation in supercooled liquids [22–25]. Further studies suggest that such elastically mediated interaction plays a key role in facilitating new rearrangements, which finally leads to the emergence of DH [26–28]. Moreover, it is also suggested that the extended-ranged elasticity is crucial in determining the nonlinear rheology of supercooled liquids [29–32]. These results open the possibility of connecting shear thinning and DH by elasticity.

Inspired by some pioneering works [19, 29], we recently proposed a concept of localized elastic region (LER) to

model the shear thinning of supercooled liquids by analyzing the distortion of $g(\mathbf{r})$ [33]. An LER is a transient zone containing hundreds of particles. It deforms elastically before yielding, which provides the resistance to the imposed shear [32–35]. In this Letter, we visualize this concept by characterizing the organization of cage jumps, i.e., large nonaffine displacements of particles [36, 37]. We find that the evolution of the localized elasticity resembles the response of amorphous solids to the start-up shear [2, 38, 39]: It sequentially undergoes elastic deformation and plastic deformation, and eventually relaxes due to the avalanche of cage jumps facilitated by the elastically mediated interaction. This relaxation process gives rise to dynamic regions that compose the major signature of DH.

Here we address the relation between DH and shear thinning by three-dimensional Brownian dynamics (BD) and molecular dynamics (MD) simulations. The BD system is the same as the one we employed before [33]: a binary mixture of $N_s = 4000$ small particles and $N_b = 16000$ big particles (diameter ratio $d_s/d_b = 2/3$) interacting via the hard-sphere Yukawa potential. The hard core is represented by the potential-free algorithm [40, 41] and the Yukawa part is expressed as $V(r) = K \frac{\exp[-z(r-d_{ij})]}{r/d_{ij}}$ for $r \geq d_{ij} \equiv (d_i + d_j)/2$, where d_i is the diameter of particle i , and the parameters $z = 4.86/d_b$ and $K = 9.69k_B T$ are determined from neutron scattering results of a charged colloidal suspension [42]. Lees-Edwards boundary condition is applied for the shear geometry with the stream velocity along the x direction and the velocity gradient along the y direction. Two volume fractions of particles, $\phi = 45\%$ and 42.5% , are adopted. More details of BD setup are given in Ref. [33]. For MD, we simulate the Kob-Andersen liquid [43] at a temperature slightly higher than the mode-coupling temperature [44] using LAMMPS [45]. In following parts, we will discuss based on the BD results. The units of length and time are, respectively, set by d_b and $\tau_0 = d_b^2/D_0$ where D_0 is the Stokes-Einstein self-diffusion coefficient. Details and results of the MD simulation are given in the Supplemen-

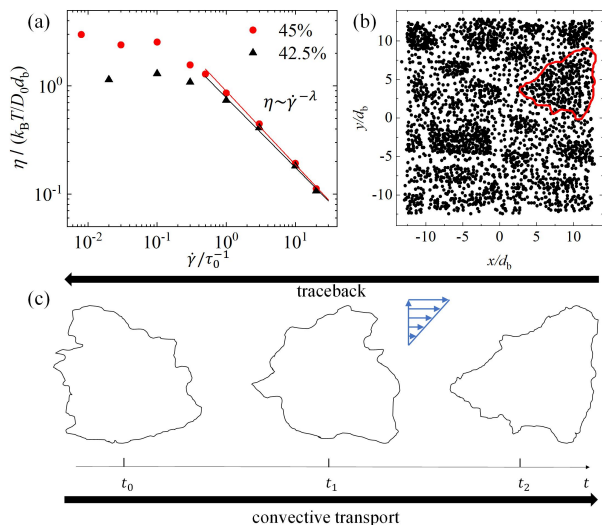


FIG. 1. (a) Shear viscosity contributed by the Yukawa potential between big particles for $\phi = 45\%$ and 42.5% BD samples. Solid lines denote fits with $\dot{\gamma}^{-\lambda}$ in the shear-thinning regime. (b) Projection of cage-jump events in the shear plane accumulated within a time interval t_χ for the $\phi = 45\%$ sample at $\dot{\gamma}\tau_0 = 3$. The red curve is the boundary of one cluster. (c) Convective transport (time-evolution) and traceback (time-reversal) of the boundary of the cluster highlighted in (b).

tal Material (SM) [46].

Figure 1(a) shows the shear thinning of BD samples calculated by $\eta = -\langle \sum_i r_{i,x} f_{i,y} \rangle / V \dot{\gamma}$, where r_i and f_i denote the position of particle i and the deterministic force exerted on particle i , respectively, and V is the system volume. Here, we only consider the interactions between big particles, because they contribute to more than 80% of the total viscosity [33]. At $\dot{\gamma}\tau_0 \geq 1$, a power-law thinning $\eta \sim \dot{\gamma}^{-\lambda}$ is present. To explore the DH in flow, we seek for the irreversible nonaffine displacements of big particles by identifying cage jumps following Candelier et al. [36, 37]. Figure 1(b) shows a projection of cage-jump events accumulated within a time interval t_χ for the $\phi = 45\%$ sample at $\dot{\gamma}\tau_0 = 3$, where t_χ is the time at which the dynamic susceptibility $\chi_4(t)$ [47] reaches maximum. The clustering of cage jumps is clearly seen, implying the significance of DH in flow. The boundary of such dynamic region is delineated according to the density distribution of cage jumps [46], and an example is given in Fig. 1(b). In passing, including the contribution of small particles does not change the heterogeneous feature of dynamics and the delineation of dynamic regions, as well as the results discussed in following paragraphs, as shown in detail in the SM [46].

To study the formation and development of a dynamic region composed of cage jumps, we affinely trace back the deformation history of its boundary in flow, as illustrated in Fig. 1(c) [46]. From a time-forward view, the boundary undergoes a convective transport in flow. We iden-

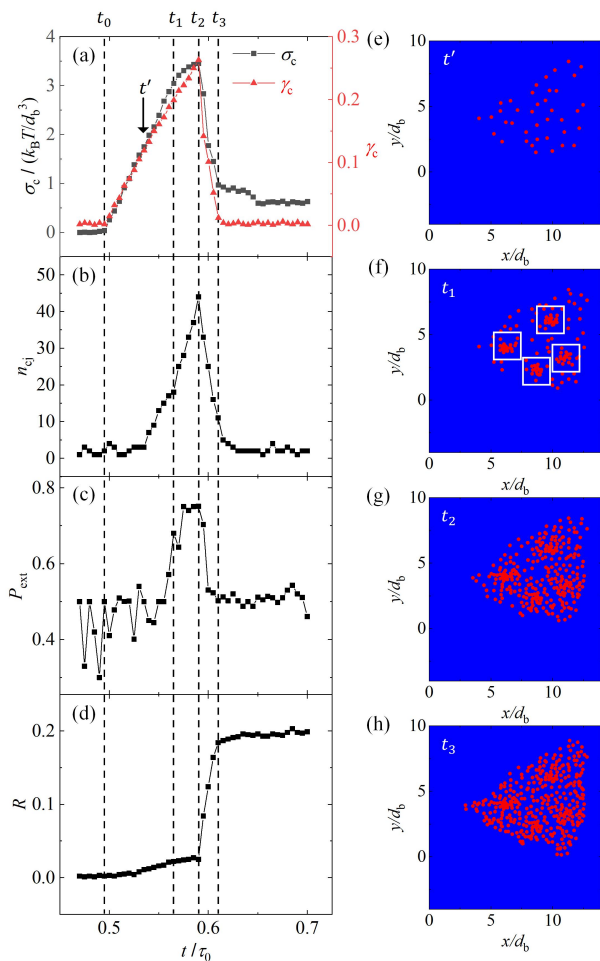


FIG. 2. Results of convective cluster analysis. Evolutions of (a) σ_c and γ_c , (b) n_{cj} , (c) P_{ext} , and (d) R of the cluster highlighted in Fig. 1(b) are shown. Characteristic moments are noted by vertical dotted lines. (e)-(h) display the spatiotemporal accumulations of cage jumps (red dots) inside the aforementioned cluster in the shear plane at t' , t_1 , t_2 and t_3 , respectively [48].

tify the big particles located inside the time-dependent boundary every Δt [49] during the traceback. Then, we calculate the shear stress σ_c of the cluster encompassed by the boundary by summing the atomic stresses of the inside big particles [50]. Figure 2(a) shows the evolution of σ_c of such a convective cluster, which finally gives rise to the dynamic region marked in Fig. 1(b). It is seen that as time t evolves, σ_c increases from nearly zero. We denote the starting point of the increase of σ_c as t_0 . At $t > t_0$, σ_c first undergoes a linear growth until t_1 , then a milder growth until t_2 , and finally a sharp drop until t_3 . In Fig. 2(a) we also show the shear strain γ_c of the cluster obtained by minimizing the mean-square local nonaffine displacement suggested by Falk and Langer [46, 51]. γ_c linearly grows with t at first, and again drops at $t = t_2$. These results suggest that the cluster sequen-

tially undergoes elastic deformation during $[t_0, t_1]$, plastic deformation during $[t_1, t_2]$, and yielding at t_2 , similar to the response of amorphous solids [2, 38, 39]. This kind of response is also found for other clusters studied in this work.

To learn more about this process, we calculate other 3 quantities. Figure 2(b) shows the temporal density of cage jumps $n_{\text{cj}}(t)$, which records the count of cage jumps in the cluster during $[t - \Delta t/2, t + \Delta t/2]$. $n_{\text{cj}}(t)$ exhibits a smooth bump at t_1 and a peak at t_2 , suggesting that the change of mechanical response is triggered by the surge of cage jumps. Previous studies [33, 38] show that irreversible displacements of particles in sheared glassy systems are mostly along the extensional direction of shear geometry. Thus, we check the direction of the displacement vector $\tilde{\mathbf{r}}_{\text{cj}}$ of every cage jump, and calculate the percentage $P_{\text{ext}}(t)$ that the projection of $\tilde{\mathbf{r}}_{\text{cj}}$ in the shear plane aligns with the 1st or the 3rd quadrant. As seen in Figure 2(c), $P_{\text{ext}}(t)$ is statistically larger than 50% during $[t_1, t_3]$ and reaches local maximum at t_1 and t_2 , which is consistent with previous results [33, 38]. Note that, though the evolution of the boundary is deterministic, the particles inside and outside the boundary can exchange. In Fig. 2(d) we characterize this exchange with $R(t) = 1 - N_{\text{res}}(t)/N_{\text{res}}(t_0)$, where $N_{\text{res}}(t)$ is the number of big particles inside the boundary at t_0 that are still inside at t . The weak exchange at $t < t_2$ suggests that the convective cluster can be viewed as an entity that evolves in a nearly closed manner. This manner is terminated by abundant rearrangements manifested by the sharp increase of $R(t)$ from t_2 .

Figure 2(e)-(h) display the spatiotemporal accumulation of cage jumps in the same cluster. At $t < t_1$, cage jumps are sparse (Fig. 2(e)). At $t \approx t_1$, a few cage jumps have concentrated on some spots with diameter of $\sim 3d_b$, as marked in Fig. 2(f). These spots are possible shear transformation zones (STZ) [51–54] as we will address later. During $[t_1, t_2]$ (Fig. 2(g)), lots of cage jumps appear throughout the cluster, stemming from the spots marked in Fig. 2(f). At $t \approx t_3$, the whole cluster has been occupied by cage jumps. The outward propagation of cage jumps from early-formed cage-jump spots shown here is consistent with the dynamic facilitation (DF) mechanism [36, 55–57].

Figure 2 illustrates how a dynamic region emerges from the yielding of a convective cluster. Next, we will establish the relation between shear thinning and convective clusters. We calculate the real-time percentage $P_c(t)$ of big particles that are included in convective clusters during a period of $3t_\chi$. Figure 3(a) shows $P_c(t)$ for the $\phi = 45\%$ sample at $\dot{\gamma}\tau_0 = 3$. It is seen that $P_c(t)$ fluctuates around its average \bar{P}_c , which is 78% in this case. \bar{P}_c slightly grows with $\dot{\gamma}$. These results suggest that most particles are participating in the deformation-yielding process of convective clusters at a given time. Thus, we expect that the shear stress of the system is

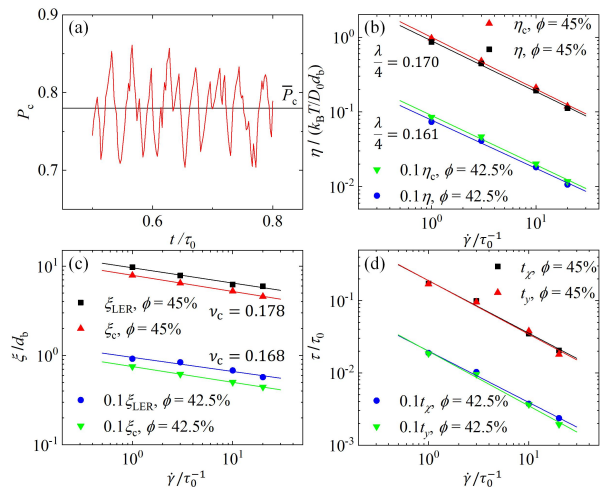


FIG. 3. (a) Percentage $P_c(t)$ of big particles inside clusters for the $\phi = 45\%$ sample at $\dot{\gamma}\tau_0 = 3$. The horizontal line gives its average value \bar{P}_c . (b) Comparison between the cluster-sustained viscosity η_c and η . Lines denote fits with $\dot{\gamma}^{-\lambda}$. (c) Comparison of the cluster radius ξ_c and the LER size ξ_{LER} . Lines denote fits with $\xi_c \sim \dot{\gamma}^{-\nu_c}$ and $\xi_{\text{LER}} \sim \dot{\gamma}^{-\nu'}$. It is seen that $\nu_c \approx \nu' \approx \lambda/4$. (d) Comparison between the yielding time t_y and t_χ . Lines denote the power-law fits.

mainly from the stress sustained by these clusters. To test this idea, we estimate the shear viscosity of the system as $\eta_c = \bar{P}_c(\sigma_{c,y}/2)\dot{\gamma}^{-1}$, where $\sigma_{c,y}$ is the average yielding stress of clusters, so that $\sigma_{c,y}/2$ is the average stress sustained by a cluster during its life cycle. In Fig. 3(b), we compare η_c with η shown in Fig. 1(a). A nice match is seen, supporting that the elasticity of convective clusters is indeed dominating in contributing the shear thinning. In Fig. 3(c), we show the average cluster radius ξ_c found by $\xi_c = (3V_c/4\pi)^{1/3}$, where V_c is the average cluster volume [58]. ξ_c shrinks with $\dot{\gamma}$ as $\xi_c \sim \dot{\gamma}^{-\nu_c}$. In our previous work [33], we propose the concept of LER within which the response to shear is elastic. The radius of LER ξ_{LER} is extracted from the spatial range of the distortion of $g(\mathbf{r})$ [33]. By applying the “solidity” picture [19, 20] to the shear condition, we find that ξ_{LER} shrinks as $\xi_{\text{LER}} \sim \dot{\gamma}^{-\nu'}$ with $\nu' \approx \lambda/4$ [33]. We also plot ξ_{LER} in Fig. 3(c). It is seen that ξ_c and ξ_{LER} behave highly consistently, with $\xi_c \approx 0.8\xi_{\text{LER}}$ for all conditions. Such consistency gives $\nu_c \approx \nu' \approx \lambda/4$, which works well as shown in Fig. 3(b) and (c). Above results demonstrate that the convective cluster is the spatiotemporal representation of the LER concept, and plays a key role in determining the nonlinear rheology. The agreement between ξ_c and ξ_{LER} is not trivial, especially considering that ξ_{LER} is found by analyzing the 2-point correlation $g(\mathbf{r})$, which is commonly considered to be not sensitive to DH features [47].

Notice that ξ_c is also the size of dynamic regions composed of cage jumps. Thus, the relation $\nu_c \approx \lambda/4$ links

DH to shear thinning through localized elasticity. To further elucidate this picture, we compare t_χ with the yielding time $t_y = \langle t_2 - t_0 \rangle$ averaged over clusters. As shown in Fig. 3(d), t_χ nicely agrees with t_y . This result, together with Fig. 2, shows that the emergence of prominent DH is intimately correlated with the massive yielding of elastic clusters.

Above discussion highlights the importance of understanding the microscopic mechanism of the yielding of convective clusters in modeling shear thinning. Considering the similarity between the responses of convective clusters and amorphous solids to shear, one may expect that the yielding of clusters is initiated by STZ. STZ is known to relate to the undeformed configuration [59]. To seek for STZs, we isolate the cluster found in Fig. 1(b), and calculate the pseudoharmonic modes (PHM) [60] with reference to its inherent structure at t_0 . In Fig. 4(a), we show the modes that indicate potential STZs in the cluster. The aggregation of these eigenvectors is featured by the geometry consistent to the shear: extensional in the 1st and the 3rd quadrant, and compressional in the other two. The cage jumps happening during $[t_0, t_1]$ are also plotted. The cage jumps spots marked in Fig. 2(f) coincide the loci of STZs predicted by PHM analysis. The emergence of STZ inside convective clusters suggests that the dynamics of sheared supercooled liquids manifests an interesting spatial hierarchy of *liquidlike background* — *solidlike medium (LER)* — *liquidlike spots (STZ)* from large length scale to small length scale.

Local plastic events trigger quadrupolar stress correlation in surrounding elastic medium [62]. This mechanism, which has been incorporated into elastoplastic models for the rheology of amorphous solids [28], was introduced to study the DH in equilibrium supercooled liquids by means of DF recently [26, 27]. The development of cage jumps shown in Fig. 2(e)-(h) exhibits DF-like feature. To clarify the relation between the localized elasticity and the likely DF, for a specific convective cluster, we calculate the pair correlation of cage jumps as [26]:

$$g_{cj}(\mathbf{r}) = \frac{N'_s}{N_b} \left\langle \sum_{j,k} \delta(\mathbf{r} - [\mathbf{r}_{s,k}(t_1 : t_2) - \mathbf{r}_{c,j}(t_1)]) \right\rangle \quad (1)$$

where $\mathbf{r}_{c,j}(t_1)$ denotes the position of the j^{th} cage jump appearing within $[t_1 - \Delta t/2, t_1 + \Delta t/2]$ inside the cluster, $\mathbf{r}_{s,k}(t_1 : t_2)$ denotes the position of the k^{th} cage jump appearing within $[t_1, t_2]$ in the whole system, and N'_s is the count of cage jumps appearing within $[t_0, t_1]$ in the whole system. $g_{cj}(\mathbf{r})$ evaluates the facilitation effect during $[t_1, t_2]$, within which massive cage jumps emerge. Figure 4(b) gives the orientation-averaged $g_{cj}(r)$ for the $\phi = 45\%$ sample. It is seen that $g_{cj}(r)$ is not sensitive to $\dot{\gamma}$. Considering the anisotropy of the strain field of plastic events, it is the anisotropy of $g_{cj}(\mathbf{r})$,

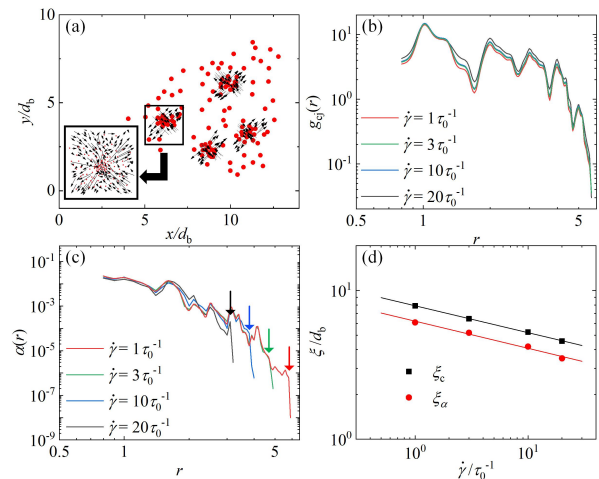


FIG. 4. (a) Projection of PHM in the shear plane for the cluster highlighted in Fig. 1(b). Cage jumps happening during $[t_0, t_1]$ are also shown. The inset is the enlarged view of the spot surrounded by the rectangle [61]. The coincidence between PHM-predicted STZs and cage-jump spots is seen. (b) and (c) respectively show the orientation-averaged $g_{cj}(r)$ and the anisotropic factor $\alpha(r)$ of the $\phi = 45\%$ sample at different $\dot{\gamma}$. The arrows in panel (c) denote the truncation radius of $\alpha(r)$. (d) Comparison between the radius of $\alpha(r)$ ξ_α and the cluster radius ξ_c . Lines denote the power-law fits.

rather than the orientation-averaged radial feature, that better measures the elastic component of $g_{cj}(\mathbf{r})$ [26]. Thus, we calculate the anisotropic factor of $g_{cj}(\mathbf{r})$ by $\alpha(r) = \langle [g_{cj}(\mathbf{r})/g_{cj}(r) - 1]^2 \rangle_\Omega$, where $\langle \dots \rangle_\Omega$ represents average over solid angle. As seen in Fig. 4(c), the amplitude of $\alpha(r)$ does not depend on $\dot{\gamma}$, whereas its spatial range clearly shrinks with $\dot{\gamma}$. We identify the truncation radius of $\alpha(r)$ (ξ_α) by the point at which $\alpha(r)$ undergoes a sudden change to a much steeper profile, as denoted by arrows in Fig. 4(c). Figure 4(d) displays the result of ξ_α , ξ_c is also plotted for comparison. ξ_α and ξ_c are seen to be highly consistent to each other, manifested by $\xi_\alpha \approx 0.8\xi_c$. This agreement confirms the localized nature of the transient elasticity, and highlights the role of elastically mediated interaction in facilitating the avalanche of cage jumps and the yielding of convective clusters.

In summary, we demonstrate the intermediate role of localized elasticity in connecting DH and shear thinning: It is the major source of viscosity that shear-thins, and its yielding gives rise to dynamic regions that constitute the prominent manifestation of DH. The yielding of the localized elasticity is initiated by STZs and facilitated by elastically mediated interaction. These observations, together with previous related studies [19–21, 26, 27, 29, 33], highlight the importance of the “hard” regions, such as LER, in governing the flow of supercooled liquids. On the other hand, for the deformation of amorphous materials, most investigations on DH fo-

cus on “soft” regions [13, 16, 51–53, 59]. By shifting the focus to the “hard” region, and establishing the firm relation between the yielding of localized elasticity and the clustering of cage jumps, we find a simple scaling law $\nu_c \approx \lambda/4$ that relates the characteristic length of DH to shear thinning.

Above conclusions are also found in the MD data, as we show in detail in the SM [46]. Particularly, the numerical agreement between ν_c and $\lambda/4$, and that between ξ_α and ξ_c , are even better than those of BD results.

This research was supported by the National Natural Science Foundation of China (No. 11975136). The Center of High Performance Computing, Tsinghua University is acknowledged for computational resources.

* Corresponding author: zwang2017@mail.tsinghua.edu.cn

- [1] R. G. Larson, *The structure and rheology of complex fluids* (Oxford University Press, New York, 1999).
- [2] P. Oswald, *Rheophysics: The Deformation and Flow of Matter* (Cambridge University Press, Cambridge, 2014).
- [3] W.-T. Ashurst and W. Hoover, Dense-fluid shear viscosity via nonequilibrium molecular dynamics, *Phys. Rev. A* **11**, 658 (1975).
- [4] J. Schwarzl and S. Hess, Shear-flow-induced distortion of the structure of a fluid: Application of a simple kinetic equation, *Phys. Rev. A* **33**, 4277 (1986).
- [5] M. Fuchs and M. E. Cates, Theory of nonlinear rheology and yielding of dense colloidal suspensions, *Phys. Rev. Lett.* **89**, 248304 (2002).
- [6] J. M. Brader, M. E. Cates, and M. Fuchs, First-principles constitutive equation for suspension rheology, *Phys. Rev. Lett.* **101**, 138301 (2008).
- [7] K. Miyazaki, D. R. Reichman, and R. Yamamoto, Supercooled liquids under shear: Theory and simulation, *Phys. Rev. E* **70**, 011501 (2004).
- [8] A. Furukawa, Onset of shear thinning in glassy liquids: Shear-induced small reduction of effective density, *Phys. Rev. E* **95**, 012613 (2017).
- [9] A. Furukawa, Quantification of the volume-fraction reduction of sheared fragile glass-forming liquids and its impact on rheology, *Phys. Rev. Res.* **5**, 023181 (2023).
- [10] H. Mizuno, A. Ikeda, T. Kawasaki, and K. Miyazaki, Universal mechanism of shear thinning in supercooled liquids, *Commun. Phys.* **7**, 199 (2024).
- [11] T. S. Ingebrigtsen and H. Tanaka, Structural predictor for nonlinear sheared dynamics in simple glass-forming liquids, *Proc. Natl. Acad. Sci. U.S.A.* **115**, 87 (2018).
- [12] T. Yamaguchi, Stress-structure coupling and nonlinear rheology of lennard-jones liquid, *J. Chem. Phys.* **148** (2018).
- [13] R. Yamamoto and A. Onuki, Dynamics of highly supercooled liquids: Heterogeneity, rheology, and diffusion, *Phys. Rev. E* **58**, 3515 (1998).
- [14] H. Mizuno and R. Yamamoto, Dynamical heterogeneity in a highly supercooled liquid under a sheared situation, *J. Chem. Phys.* **136** (2012).
- [15] A. Furukawa, K. Kim, S. Saito, and H. Tanaka, Anisotropic cooperative structural rearrangements in sheared supercooled liquids, *Phys. Rev. Lett.* **102**, 016001 (2009).
- [16] V. Lubchenko, Shear thinning in deeply supercooled melts, *Proc. Natl. Acad. Sci. U.S.A.* **106**, 11506 (2009).
- [17] M. D. Ediger, Spatially heterogeneous dynamics in supercooled liquids, *Annu. Rev. Phys. Chem.* **51**, 99 (2000).
- [18] C. P. Royall and S. R. Williams, The role of local structure in dynamical arrest, *Phys. Rep.* **560**, 1 (2015).
- [19] J. C. Dyre, Colloquium: The glass transition and elastic models of glass-forming liquids, *Rev. Mod. Phys.* **78**, 953 (2006).
- [20] J. C. Dyre, Solidity of viscous liquids, *Phys. Rev. E* **59**, 2458 (1999).
- [21] J. C. Dyre, Solid-that-flows picture of glass-forming liquids, *J. Phys. Chem. Lett.* **15**, 1603 (2024).
- [22] A. Lemaître, Structural relaxation is a scale-free process, *Phys. Rev. Lett.* **113**, 245702 (2014).
- [23] B. Illing, S. Fritschi, D. Hajnal, C. Klix, P. Keim, and M. Fuchs, Strain pattern in supercooled liquids, *Phys. Rev. Lett.* **117**, 208002 (2016).
- [24] V. A. Levashov, J. R. Morris, and T. Egami, Viscosity, shear waves, and atomic-level stress-stress correlations, *Phys. Rev. Lett.* **106**, 115703 (2011).
- [25] H. Tong, S. Sengupta, and H. Tanaka, Emergent solidity of amorphous materials as a consequence of mechanical self-organisation, *Nat. Commun.* **11**, 4863 (2020).
- [26] R. N. Chacko, F. P. Landes, G. Biroli, O. Dauchot, A. J. Liu, and D. R. Reichman, Elastoplasticity mediates dynamical heterogeneity below the mode coupling temperature, *Phys. Rev. Lett.* **127**, 048002 (2021).
- [27] M. Ozawa and G. Biroli, Elasticity, facilitation, and dynamic heterogeneity in glass-forming liquids, *Phys. Rev. Lett.* **130**, 138201 (2023).
- [28] A. Nicolas, E. E. Ferrero, K. Martens, and J.-L. Barrat, Deformation and flow of amorphous solids: Insights from elastoplastic models, *Rev. Mod. Phys.* **90**, 045006 (2018).
- [29] T. Iwashita and T. Egami, Atomic mechanism of flow in simple liquids under shear, *Phys. Rev. Lett.* **108**, 196001 (2012).
- [30] J. Chattoraj and A. Lemaître, Elastic signature of flow events in supercooled liquids under shear, *Phys. Rev. Lett.* **111**, 066001 (2013).
- [31] A. Ghosh and K. S. Schweizer, The role of collective elasticity on activated structural relaxation, yielding, and steady state flow in hard sphere fluids and colloidal suspensions under strong deformation, *J. Chem. Phys.* **153** (2020).
- [32] P. Sollich, F. Lequeux, P. Hébraud, and M. E. Cates, Rheology of soft glassy materials, *Phys. Rev. Lett.* **78**, 2020 (1997).
- [33] D. Kong, W.-R. Chen, K.-Q. Zeng, L. Porcar, and Z. Wang, Localized elasticity governs the nonlinear rheology of colloidal supercooled liquids, *Phys. Rev. X* **12**, 041006 (2022).
- [34] D. J. Lacks, Energy landscapes and the non-newtonian viscosity of liquids and glasses, *Phys. Rev. Lett.* **87**, 225502 (2001).
- [35] S. Patinet, D. Vandembroucq, and M. L. Falk, Connecting local yield stresses with plastic activity in amorphous solids, *Phys. Rev. Lett.* **117**, 045501 (2016).
- [36] R. Candelier, O. Dauchot, and G. Biroli, Building blocks of dynamical heterogeneities in dense granular media, *Phys. Rev. Lett.* **102**, 088001 (2009).
- [37] R. Candelier, A. Widmer-Cooper, J. K. Kummerfeld,

- O. Dauchot, G. Biroli, P. Harrowell, and D. R. Reichman, Spatiotemporal hierarchy of relaxation events, dynamical heterogeneities, and structural reorganization in a supercooled liquid, *Phys. Rev. Lett.* **105**, 135702 (2010).
- [38] N. Koumakis, M. Laurati, S. Egelhaaf, J. Brady, and G. Petekidis, Yielding of hard-sphere glasses during start-up shear, *Phys. Rev. Lett.* **108**, 098303 (2012).
- [39] M. Laurati, P. Maßhoff, K. J. Mutch, S. U. Egelhaaf, and A. Zaccone, Long-lived neighbors determine the rheological response of glasses, *Phys. Rev. Lett.* **118**, 018002 (2017).
- [40] D. R. Foss and J. F. Brady, Brownian dynamics simulation of hard-sphere colloidal dispersions, *J. Rheol.* **44**, 629 (2000).
- [41] D. Heyes and J. Melrose, Brownian dynamics simulations of model hard-sphere suspensions, *J. Non-Newtonian Fluid Mech.* **46**, 1 (1993).
- [42] Z. Wang, T. Iwashita, L. Porcar, Y. Wang, Y. Liu, L. E. Sánchez-Díaz, B. Wu, G.-R. Huang, T. Egami, and W.-R. Chen, Local elasticity in nonlinear rheology of interacting colloidal glasses revealed by neutron scattering and rheometry, *Phys. Chem. Chem. Phys.* **21**, 38 (2019).
- [43] W. Kob and H. C. Andersen, Testing mode-coupling theory for a supercooled binary lennard-jones mixture i: The van hove correlation function, *Phys. Rev. E* **51**, 4626 (1995).
- [44] For this system, the mode-coupling temperature is 0.435 in Lennard-Jones unit. The temperature we adopt is 0.45.
- [45] A. P. Thompson, H. M. Aktulga, R. Berger, D. S. Bolinteanu, W. M. Brown, P. S. Crozier, P. J. In't Veld, A. Kohlmeyer, S. G. Moore, T. D. Nguyen, *et al.*, LAMMPS—a flexible simulation tool for particle-based materials modeling at the atomic, meso, and continuum scales, *Comput. Phys. Commun.* **271**, 108171 (2022).
- [46] See the Supplemental Material at ... for details of simulation, calculations, and MD results.
- [47] N. Lačević, F. W. Starr, T. Schröder, and S. C. Glotzer, Spatially heterogeneous dynamics investigated via a time-dependent four-point density correlation function, *J. Chem. Phys.* **119**, 7372 (2003).
- [48] Coordinates of cage-jump events plotted in Fig. 2(e)-(h) have been transformed to the moment of maximum χ_4 by affine displacements of the convective shear, in order to compare between different moments. (.)
- [49] $\Delta t = 0.005\tau_0$ for $\dot{\gamma} = 1\tau_0^{-1}$ and $3\tau_0^{-1}$; $\Delta t = 0.002\tau_0$ for $\dot{\gamma} = 10\tau_0^{-1}$; $\Delta t = 0.001\tau_0$ for $\dot{\gamma} = 20\tau_0^{-1}$.
- [50] T. Egami, Atomic level stresses, *Prog. Mater. Sci.* **56**, 637 (2011).
- [51] M. L. Falk and J. S. Langer, Dynamics of viscoplastic deformation in amorphous solids, *Phys. Rev. E* **57**, 7192 (1998).
- [52] A. Argon, Plastic deformation in metallic glasses, *Acta Metall.* **27**, 47 (1979).
- [53] P. Schall, D. A. Weitz, and F. Spaepen, Structural rearrangements that govern flow in colloidal glasses, *Science* **318**, 1895 (2007).
- [54] Y. Fan, T. Iwashita, and T. Egami, How thermally activated deformation starts in metallic glass, *Nat. Commun.* **5**, 5083 (2014).
- [55] D. Chandler and J. P. Garrahan, Dynamics on the way to forming glass: Bubbles in space-time, *Annu. Rev. Phys. Chem.* **61**, 191 (2010).
- [56] A. S. Keys, L. O. Hedges, J. P. Garrahan, S. C. Glotzer, and D. Chandler, Excitations are localized and relaxation is hierarchical in glass-forming liquids, *Phys. Rev. X* **1**, 021013 (2011).
- [57] C. Scalliet, B. Guiselin, and L. Berthier, Thirty milliseconds in the life of a supercooled liquid, *Phys. Rev. X* **12**, 041028 (2022).
- [58] We calculate the radius of gyration tensor for clusters. The eigenvalue analysis shows that the average ratio of the largest and smallest eigenvalues is 1.26 at $t = t_0$, suggesting that clusters at $t = t_0$ are not very asymmetric and, thus, using the effective radius to evaluate the cluster size is acceptable.
- [59] D. Richard, M. Ozawa, S. Patinet, E. Stanifer, B. Shang, S. Ridout, B. Xu, G. Zhang, P. Morse, J.-L. Barrat, *et al.*, Predicting plasticity in disordered solids from structural indicators, *Phys. Rev. Mater.* **4**, 113609 (2020).
- [60] D. Richard, G. Kapteijns, J. A. Giannini, M. L. Manning, and E. Lerner, Simple and broadly applicable definition of shear transformation zones, *Phys. Rev. Lett.* **126**, 015501 (2021).
- [61] In the main part of Fig. 4(a), only PHM projections with significant magnitude are retained for clarity. the inset of Fig. 4(a) shows all PHM projections surrounding the highlighted cage-jump spot. (.)
- [62] G. Picard, A. Ajdari, F. Lequeux, and L. Bocquet, Elastic consequences of a single plastic event: A step towards the microscopic modeling of the flow of yield stress fluids, *Eur. Phys. J. E* **15**, 371 (2004).